Supporting Information for "Effect of Surface Energy on Size-Dependent Deformation Twinning of Defect-Free Au Nanowires"

Byungil Hwang‡[1], Mijeong Kang‡[2], Subin Lee[3], Christopher R. Weinberger[4], Phillip Loya[5], Jun Lou[5], Sang Ho Oh[3], Bongsoo Kim*[2], and Seung Min Han*[1].

1. Graduate School of Energy Environment Water and Sustainability, Korea Advanced Institute of Science & Technology, Daejeon, Republic of Korea, 305-701

2. Department of Chemistry, Korea Advanced Institute of Science & Technology, Daejeon, Republic of Korea, 305-701

3. Department of Materials Science and Engineering, Pohang University of Science and Technology (POSTECH), Pohang, Republic of Korea, 790-784

4. Department of Mechanical Engineering and Mechanics, Drexel University, Philadelphia, USA, PA 19104

5. Department of Materials Science and Nano Engineering, Rice University, Houston, USA, TX 77005.

Corresponding Author: smhan01@kaist.ac.kr, bongsoo@kaist.ac.kr

1

Supporting Information 01.

The theoretical model by Chen et al. was then modified by Sedlmayr et al.[1] to consider the contribution from different Schmid factors for full and partial dislocations, and can be written as

$$D_c = \frac{2\alpha\mu\left(b_N \cdot \frac{m_{lp}}{m} - b_p\right)b_p}{\gamma_{SF}} \ (4),$$

where m and m_{lp} is the Schmid factors for perfect and leading partial dislocations, respectively. μ is the shear modulus, γ_{SF} is the stacking fault energy, and b_N and b_P are the magnitudes of the Burgers vectors of the perfect dislocation and the partial dislocation, respectively. Alpha (α) is the parameter about the character of the dislocation (0.5 and 1.5 for edge and screw dislocations, respectively. This model prediction for the Au nanowire results in critical size of ~33 nm, below which twin deformation will occur in Au nanowires. If we additionally account for the differences in surface energies when twin deformation occurs in nanowires, the critical diameter is increased further from 33 nm to 36 nm.
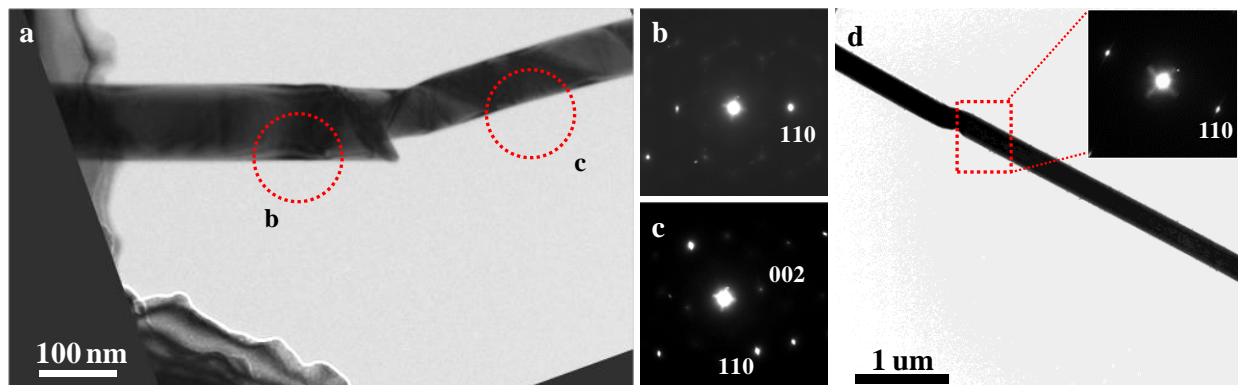
Supporting Information 02.

Fig. S2 (a) A TEM image of 102 nm Au nanowire after loading is completed and the wire is partially twinned, and (b) a SAD patterns of untwined region and (c) twinned region. (d) A TEM image of 167 nm Au nanowire and its SAD patterns taken at the deformed region demonstrating the lack of deformation twinning.

TEM images and the diffraction patterns taken from the twinned and un-twinned region of the 102 nm nanowire after twin propagation are shown in Fig. S2a-c. The untwinned section was observed at one end due to the overflowed epoxy, which was used to mount the nanowire onto the PTP device, which prevented this section from twinning. The SAD patterns indicate that the twinned region has a [100] orientation while the untwined region remains in its original crystallographic [110] orientation. For [110] gold nanowires, twin propagation is known to cause crystallographic re-orientation from the initial [110] orientation with a rhombic cross section and {111} side facets to a [100] nanowire with {100} side facets. Therefore, orientation change after deformation confirms that twin propagation was the dominant deformation mechanism in nanowires with diameters smaller than D_c.

In contrast, no axial orientation change was observed for the nanowire of 167 nm diameter after failure. Fig. S2d provides TEM image of 167 nm Au nanowire, and the SAD patterns taken at the deformed region (red square) are presented together. The Au nanowire with a 167 nm diameter

3

retained its [110] orientation without any axis change even after failure, which is indicative of the twin propagation being not prevalent in this nanowire.

Supporting Information 03.

The deformation of nanowires and nanoribbons were modeled using non-equilibrium molecular dynamics simulating a constant strain rate experiment under isothermal loading conditions using LAMMPS[2]. The Foiles EAM potential for gold[3] was used to model the interatomic forces and the equations of motion were integrated with a 1 fs time-step. A Nose-Hoover thermostat was used to control the temperature (300 K) and the nanoribbons were pulled at a constant engineering strain rate of $1e^8$ s^{-1}. The nanoribbons all have a thickness of 5 nm, and widths of 5, 10, 20 and 50 nm were studied. The corresponding lengths of nanowires were held at 5 times their width (25 nm, 50 nm, 100 nm and 250 nm), thus the largest simulation contained ~3.5 million atoms.

Detailed analysis of the dislocations in the MD simulations provides direction insight into the change from deformation twinning to dislocation slip. For <110> oriented nanowires, there are only two possible planes on which deformation twinning or can occur, the two that do not make up the free surfaces. Thus, for a [110] oriented nanowire, the free surface correspond to the $(\bar{1}11)$ and the $(1\bar{1}1)$ and the potential slip planes are the (111) and the $(11\bar{1})$. The potentially operational twin systems are $[112](11\bar{1})$ and $[11\bar{2}](111)$ and the potential slip systems include: $[1\bar{1}0](111)$, $[10\bar{1}](111)$, $[01\bar{1}](111)$ and $[101](11\bar{1})$, $[011](11\bar{1})$, $[1\bar{1}0](11\bar{1})$. The perfect slip system will leave no surface step (trace) if the dot product between the Burgers vector and the free surface is zero. Thus, the $[01\bar{1}](111)$ and the $[101](11\bar{1})$ slip systems leave no traces

on the $(\bar{1}11)$ surface and the $[10\bar{1}](111)$ and $[011](11\bar{1})$ leave no slip traces on the $(1\bar{1}1)$ free surface. Thus, there are two possible slip systems that are able to activate that leave no slip traces on one of the free surfaces. This suggests, and is demonstrated by our MD simulations, that slip is enabled by the nucleation of trailing partials to remove surface steps on the larger free surface, reducing the surface energy of the material. Thus, the removal of the surface steps changes the energetics of trailing partial dislocation nucleation to favor trailing partials, despite the difference in Schmid factors (0.47 for leading and 0.25 for trailing partials).

Supporting Information 04.

<Before twinning> <After twinning>

l **18°** $[001]$ $l_r = \sqrt{2} \cdot l$

$[110]$

<Cross-section>

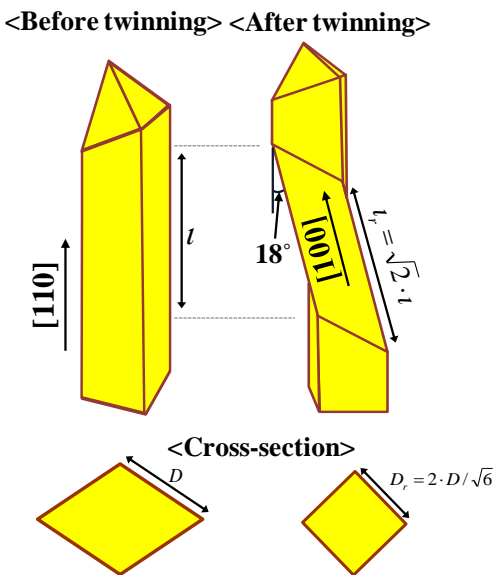D $D_r = 2 \cdot D / \sqrt{6}$

Fig. S4 Illustrations of nanowires before and after twinning

To update the diameter dependent model of Chen et al., the energy associated with surface re-orientation must be accounted for their energetic model. Here, we combine the model of Chen[4] with the model of Seo et al[5]. Upon deformation twinning, the {111} free surfaces re-orient to

{100} surfaces, and the difference in surface energies, $S_{\{100\}}$ -$S_{\{111\}}$, has to be considered in any energetic model. Since re-orientation will also cause tilt of 18.0°, the total surface area of the twinned section will also change. In addition, the length of the nanowire will elongate while the diameter is decreased within the twinned section. Therefore, the difference in surface energy, change in the total surface area as well as change in the geometry (length and diameter) need to be considered simultaneously, and this was previously derived in the work by Seo et al. that is briefly described here again. As can be seen in Fig. S4, the change of nanowire dimension from re-orientation can be written as $D_r = 2 \cdot D/\sqrt{6}$, and $l_r = \sqrt{2} \cdot l$, where D and l are the diameter and length of nanowire before re-orientation, and D_r and l_r are the diameter and length of nanowire after re-orientation. The applied stress to overcome the surface re-orientation by twinning was derived as $\sigma_s = \Delta S/D$,[5] where ΔS accounts for the difference in the surface energy due to re-orientation from {111} to {100}. For the transition from [110] oriented Au nanowires with {111} side surfaces to [100] oriented Au nanowires with {100} surfaces, the total surface energies of [110] oriented nanowire with [111] side surfaces, $S_{\{111\}}$, and [100] oriented with [100] surfaces, $S_{\{100\}}$ are written as

$$S_{\{111\}} = \gamma_{\{111\}} \cdot 4l \cdot D \ (1) \qquad\qquad S_{\{100\}} = \gamma_{\{100\}} \cdot l \cdot D \cdot \frac{8\sqrt{3}}{3} \ (2)$$

where $\gamma_{\{100\}}$ and $\gamma_{\{111\}}$ are the surface energies for {100} and {111} surfaces, respectively. Since difference in total surface energy has to be equal to the work done by the applied force,

$F\Delta l = S_{\{100\}} - S_{\{111\}}$, and the applied force along the nanowire can be written as

$$F = \frac{S_{\{100\}} - S_{\{111\}}}{\Delta l} \ (3)$$

Δl is the change of length before and after re-orientation, which is $\Delta l = l_r - l = (\sqrt{2} - 1) \cdot l$.

Therefore, the stress of surface re-orientation can be written as

$$\sigma_S = \frac{F}{A_{100}} = \frac{S_{\{100\}}-S_{\{111\}}}{\Delta l \cdot A_{100}} = \frac{4\sqrt{3}(\gamma_{100}-\frac{\sqrt{3}}{2}\gamma_{111})}{\sqrt{2}-1} \cdot \frac{1}{D} \quad (4)$$

where A_{100} is the area of cross-section of the re-oriented [100] nanowire. For convenient, we took a symbol of ΔS,

$$\Delta S = \frac{4\sqrt{3}(\gamma_{100}-\frac{\sqrt{3}}{2}\gamma_{111})}{\sqrt{2}-1} \quad (6)$$

The equation for the nucleation stress of leading partial dislocation accompanying surface re-orientation, therefore, can be obtained by adding the stress of surface re-orientation to the classical dislocation model reported in the work by Chen et al[4]. as follows,

$$\tau_{P'} = \frac{2\alpha\mu b_p}{D} + \frac{\gamma_{SF}}{b_p} + \frac{\Delta S}{D} \quad (7)$$

The critical diameter for the transition of deformation mechanism from ordinary dislocation plasticity to deformation twinning can be defined as the diameter, in which $\tau_N - \tau_{p'} = 0$, and thus, the new analytical model to calculate the critical diameter can be written as

$$\tau_N - \tau_{p'} = \left(\frac{2\alpha\mu b_N}{D}\right) - \left(\frac{2\alpha\mu b_p}{D} + \frac{\gamma_{SF}}{b_p} + \frac{\Delta S}{D}\right) = 0$$

$$D_{c'} = \frac{2\alpha\mu(b_N-b_p)b_p - \Delta S \cdot b_p}{\gamma_{SF}} \quad (8)$$

The new analytical model, eq (8), was then modified by considering the contribution from different Schmid factors for the nucleation of full and partial dislocations as suggested by Sedlmayr et al.,[1] and can be written as

$$D_{c''} = \frac{2\alpha\mu\left(b_N \cdot \frac{m_{lp}}{m} - b_p\right)b_p - \Delta S \cdot b_p \cdot m_{lp}}{\gamma_{SF}} \ (9),$$

where m and m_{lp} is the Schmid factors for perfect and leading partial dislocations, respectively.

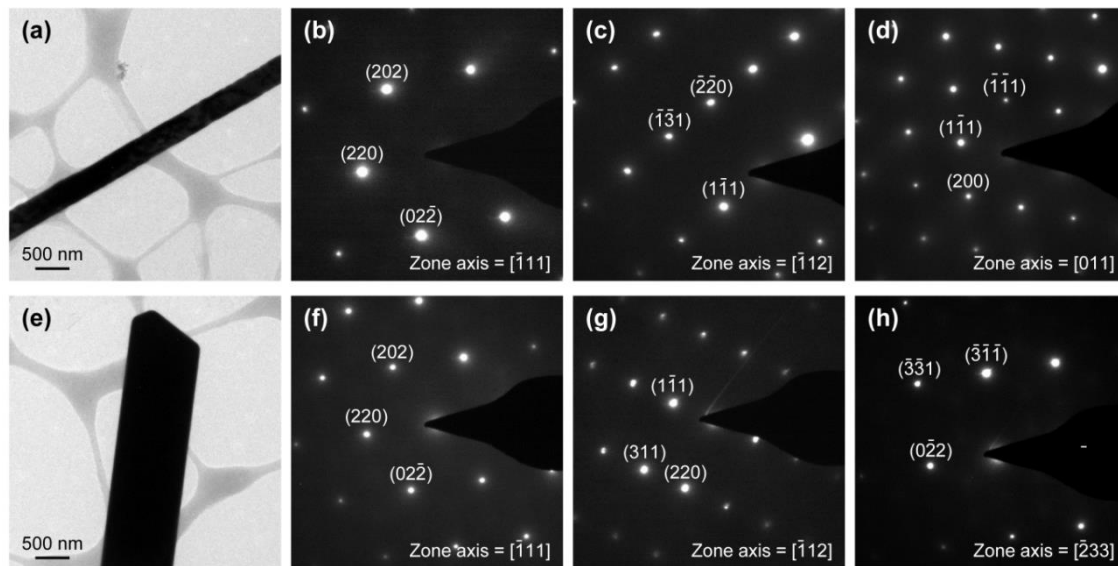**Supporting Information 05.**

Fig. S5. Transmission electron microscope images and selected area diffraction (SAD) patterns of a Au nanowire (a-d) and nanoribbon (e-h). The SAD patterns were obtained at different zone axes by rotating the nanowire or the nanoribbon along their long axes.
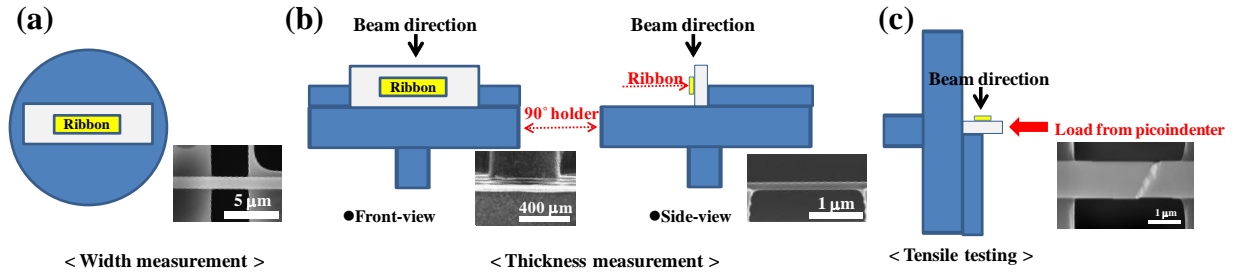
Supporting Information 06.

Fig. S6 Schematics of the process to measure the thickness of nanoribbons.

Fig. S6 shows how the dimensions (width and thickness) of the Au nanowires/ribbons were measured. Before performing tensile tests, Au nanowires/ribbons was mounted on the push-to-pull (PTP) device and placed on a typical plan-view and cross section (90 degree) SEM holders to image the width and the thickness, respectively (Fig. S6a-b). The PTP device is then loaded on the picoindenter (PI-85) to perform the tensile tests, and the width of the sample is now oriented in the e-beam direction. Thus the plan-view image is recorded while performing in-situ SEM tensile tests.
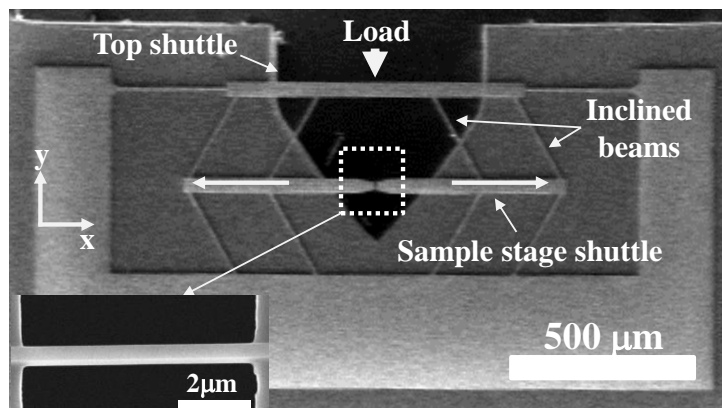
Supporting Information 07.

Fig. S7 A SEM image of the PTP device. The white arrows on the sample stage indicate the direction of the movement of the shuttles as a result of the applied load by the indenter tip at the top. (Inset) An enlarged SEM image of a clamped nanowire sample taken from the white dot square.

A SEM image of the PTP device and its components are given in Fig. S7. The Si based PTP device consists of movable sample-stage shuttles, where a metal nanowire is clamped between the two ends of the shuttles. These sample-stage shuttles are connected to the top shuttle via inclined freestanding beams, thereby translating an applied force along the y-axis from the nanoindentor into a 2-D horizontal movement of the sample-stage shuttles. The manipulation of nanowire was performed using a custom-made micromanipulator equipped with optical microscope. The freestanding gold nanowire, having a length of ~20 μm, was visible under optics due to light scattering. HARDMAN Water-Clear Epoxy was used to clamp the nanowires. The sample-stage shuttles of the PTP device was coated with a small quantity of the epoxy using a tungsten tip micromanipulator, and the nanowires were picked up using a clean manipulator and positioned across the epoxy-coated shuttles. The PTP devices with the nanowires were subsequently attached to the *in-situ* SEM/TEM holder by using silver paste.

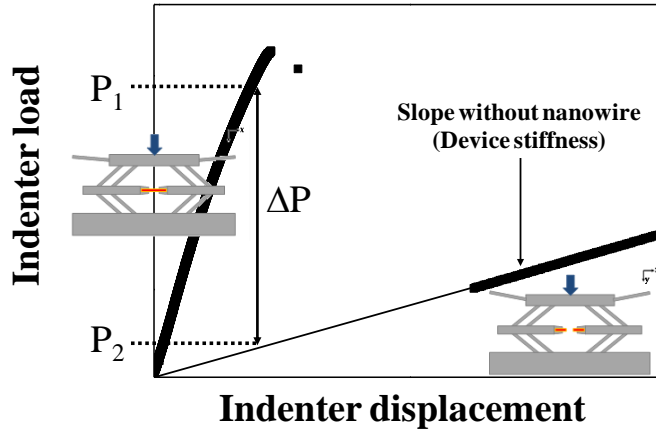**Supporting Information 08.**

Fig. S8 Typical load-displacement curve obtained from nanoindenter.

The stress-strain curves of the loading of the nanowires were derived from the nanoindenter load-displacement data with the response subtraction method, which is described in detail in the work by Y. Ganesanet al[6]. Fig. S8 presents a typical load-displace curve of the tensile tests using the PTP devices. The load, ΔP, applied to the nanowire is calculated by subtracting the load applied to the PTP device, P_2, from the total measured load, P_1. The device stiffness without nanowire is obtained from the slope of the linear region in the load-displacement curve after the nanowire fails. The obtained normal load and displacement values are then converted to lateral components by using load conversion coefficient, C_P, and displacement conversion coefficient, C_D, respectively. These coefficients are obtained from FEA simulation as a function of sample stiffness, and details can be seen in Ref [5].

References

1. A. Sedlmayr, E. Bitzek, D. S. Gianola, G. Richter, R. Mönig and O. Kraft, *Acta Mater.*, 2012, **60**, 3985-3993.

2. S. Plimpton, *J. Comput. Phys.*, 1995, **117**, 1-19.

3. D. L. Medlin, S. M. Foiles and D. Cohen, *Acta Mater.*, 2001, **49**, 3689-3697.

4. M. Chen, E. Ma, K. J. Hemker, H. Sheng, Y. Wang and X. Cheng, *Science*, 2003, **300**, 1275-1277.

5. J. H. Seo, H. S. Park, Y. Yoo, T. Y. Seong, J. Li, J. P. Ahn, B. Kim and I. S. Choi, *Nano Lett.*, 2013, **13**, 5112-5116.

6. Y. Ganesan, L. Yang, P. Cheng, L. Hao, R. Ballarini and L. Jun, *J. Microelectromech. Sys.*, 2010, **19**, 675-682.